Eur. Phys. J. E (2011) **34**: 131
DOI 10.1140/epje/i2011-11131-7

THE EUROPEAN PHYSICAL JOURNAL E

Regular Article

Dynamics of interacting edge defects in copolymer lamellae

J.D. McGraw[1], I.D.W. Rowe[1], M.W. Matsen[2], and K. Dalnoki-Veress[1,a]

[1] Department of Physics & Astronomy and the Brockhouse Institute for Materials Research, McMaster University, Hamilton, ON, Canada
[2] School of Mathematical and Physical Sciences, University of Reading, Whiteknights, Reading, UK

Received 16 August 2011
Published online: 21 December 2011 –

Abstract. It is known that terraces at the air-polymer interface of lamella-forming diblock copolymers do not make discontinuous jumps in height. Despite the underlying discretized structure, the height profiles are smoothly varying. The width of a transition region of a terrace edge in isolation is typically several hundreds of nanometres, resulting from a balance between surface tension, chain stretching penalties, and the enthalpy of mixing. What is less well known in these systems is what happens when two transition regions interact with one another. In this study, we investigate the dynamics of the interactions between copolymer lamellar edges. We find that the data can be well described by a model that assumes a repulsion between adjacent edges. While the model is simplistic, and does not include molecular level details, its agreement with the data suggests that some of the the underlying assumptions provide insight into the complex interplay between defects.

1 Introduction

Diblock copolymers are formed when two chemically distinct polymer chains, "A" and "B", are covalently bonded together. Self-assembly of these molecules into compositionally periodic structures occurs when different species of the molecules have a sufficiently unfavourable interaction energy [1]. For the simplest case in which the molecules' A and B blocks are roughly the same size, a lamellar morphology is observed. Within the lamellae of a well-ordered system, the periodic change in the concentration of a given chemical species depends on the size of the molecule. The repeat period has a well-defined value, H_o, and each lamella consists of a bilayer of molecules: $A-B/B-A$. The characteristic lengthscale of the morphology given by H_o is the result of a balance between an enthalpic repulsion of the A and B blocks, and the entropy which favours a random coil configuration. The repeat period of the bilayers is on the order of the radius of gyration of the molecule (~ 10 nm) and is controlled by the product χN; where N is the number of monomers in the polymer chain and χ is the Flory-Huggins parameter which defines the chemical incompatibility of the A and B segments [2]. Similarly, the degree of ordering is also determined by χN. Values of χN much greater than 10 lead to strong segregation of the blocks, with the $A-B$ junction points of the diblocks confined to nearly two-dimensional planes. χ is a decreasing function of the temperature since the degree of order must also decrease with temperature. When χN decreases, the junctions make increasingly greater excursions from their strongly confined two-dimensional planes until finally all order is lost in passing through the order disorder transition (ODT). More exotic morphologies can be observed when the lengths of the two blocks differ, thereby encouraging curvature at the interfaces [1,3].

Diblock copolymers serve as model systems for studying self-assembly, with promise for data storage [4,5], adhesion [6], and photonics applications [7], among others [7]. The phase behaviour and morphology of these systems in the bulk is well established both theoretically and experimentally [1,8–12]. However, when confinement dimensions approach those of the micro-phase separation, novel structures emerge. In such cases, the molecules pay an energy penalty in conforming to the geometry of confinement. Furthermore, it is typical for there to be a preference for either the A or B block to contact the confining interface. The preferential interaction can provide further frustration from the ideal bulk morphology and even induce order at temperatures above the bulk ODT [13–17]. Confinement of a diblock copolymer by a non-deformable interface has been termed *hard confinement*. Such systems have received much attention, resulting in a rich variety of phases that have been predicted and observed for systems under planar, cylindrical and spherical confinement [7,18–23].

Soft confinement of diblock copolymer systems, where the confining interface itself may deform as a result of the underlying diblock morphology, reveals an additional complexity to the interplay between the optimal bulk mor-

[a] e-mail: dalnoki@mcmaster.ca

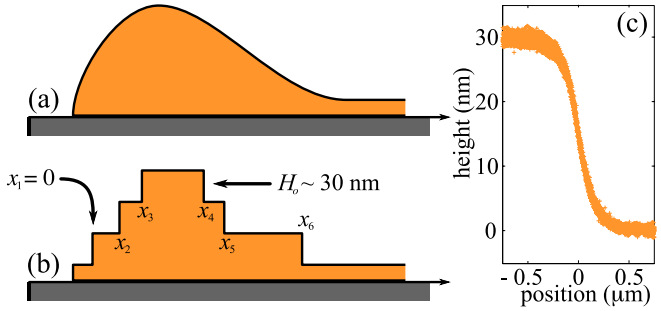

Fig. 1. Schematic cross-section of a) an as-prepared ring, and b) its condition upon annealing for a short period of time. The positions, x_i, of lamellar edges for a stack with 3 bilayers ($n = 6$) are also shown schematically; in this study, $x_n - x_1 \sim 7\,\mu$m is typical. c) AFM topography line profiles of isolated edges.

phology and the interface. Perhaps the simplest example of soft confinement is provided by the free interface of a thin symmetric diblock film supported on a substrate. In such a case the hard confinement of the substrate will typically show a preference for one of the blocks which orients the lamellae parallel to the substrate. However, the soft free interface is able to deform to minimize the free energy of the system which has a profound effect on the morphology of the air-polymer interface [24, 25]. For the case of a lamellae-forming diblock, the ability of the free surface to accommodate the layers can result in a terraced height profile, with steps in the height of the film that correspond to a molecular bilayer with height H_o.

To understand the formation of terraces on the free surface, take for example a diblock film with thickness h under *symmetric wetting* conditions (the substrate and free interface favour the same block). In the ordered state, the ideal thickness at any point in the film is commensurate with an integer number of bilayers, $h = kH_o$, where k is an integer. That is, a continuously varying topography will develop into a terraced free surface upon ordering. The transition from continuously varying topography to a terraced height profile is shown in figs. 1a) and b) for the *asymmetric wetting* case. For asymmetric wetting, the substrate and free surface favour the opposite species. In this case there exists an additional diblock *monolayer* at the substrate to satisfy the wetting condition of A at one interface and B at the other [25]. Asymmetric wetting is observed in the work discussed here and illustrated by the nearest-to-substrate monolayer shown in fig. 1b).

Away from the transition region where the topography changes by one lamellar step, the preferred lamellar spacing, H_o, is the result of an interplay between the chain stretching and interfacial energies [2]. However, in the transition from one terrace to the next, a discrete step function results in a significant cost to the free energy because of the excess surface area. Instead the transition region is broadened by the Laplace pressure. Thus, a larger surface tension will result in a broader transition. The detailed shape and morphology of the transition between terraces has been studied by several groups in the past decades [26–29]. It has been found that the transition region can induce a number of different morphologies depending on the polymer and substrate combination as the underlying equilibrium morphology is frustrated by the non-ideal confinement of the interface. The internal structure can be a dislocation [26,27], lamellae oriented perpendicular to the interface [28], and cylindrical domains [29]. The morphology of asymmetric diblock copolymer liquids which favour morphologies more complex than lamellae can also be affected by the thickness gradient in the transition region [30].

In fig. 1c) is shown an atomic force microscopy (AFM) measurement of the topography of several lamellar transition regions in a poly(styrene-methyl methacrylate) (PS-PMMA) thin film. While the experimental details are described below, it is immediately clear that the edge is not discontinuous, but is smoothly varying. The resulting topography is an edge defect with a cost to the free energy of the system that is minimised by an interplay between the interfacial and stretching energies as discussed above. Recent studies by Croll and coworkers [31] and Kim and Matsen [32] have investigated the detailed shape of symmetric diblock copolymer droplets in the ordered state. It was found that when the distance between two edges becomes small, there is an interaction between the defects. In the work by Croll and coworkers, AFM images revealed that the droplets self-assemble into a nearly conical shape of terraced disks reminiscent of Mayan temples. The shape of the droplets was understood in terms of a model which included a repulsive interaction between the edges.

Qualitatively, the origin of the repulsive interaction is easily understood. As two edges, each with an equilibrium height profile similar to that shown in fig. 1c) approach each other, their shapes must change from ideal which results in an energy penalty. In [31] an empirical, exponentially decaying, repulsive interaction was found to give good agreement with the experiments; however, the agreement was not sensitive to the exact functional form of the interaction. Furthermore, while the morphologies of diblock droplets were remarkable, the cylindrically symmetric geometry results in a complexity not related to the edge interaction alone. Specifically, the disks which make up the droplet have curvature, resulting in an *edge tension* contribution to the free energy that scales linearly with the radius of the disk. The equilibrium nature of the study and dependence on edge tension resulted in an inherent insensitivity to the functional form of the defect interaction [31].

With a view towards gaining a more general understanding of the interaction between topological defects we focus here on the dynamics of the interplay between the transition region in a simplified geometry. We have recently learned to prepare polymer tori on a substrate [33]. These structures form much like a nanoscale version of a rim left behind by an evaporating droplet, *e.g.* the stain left behind by a coffee spill [34–36]. These rings are not perfect tori: upon preparation the cross-section of the ring is asymmetric and also forms a very thin layer interior to the ring as shown by the schematic in fig. 1 [33]. If the rings are prepared so that they are thin but have a large

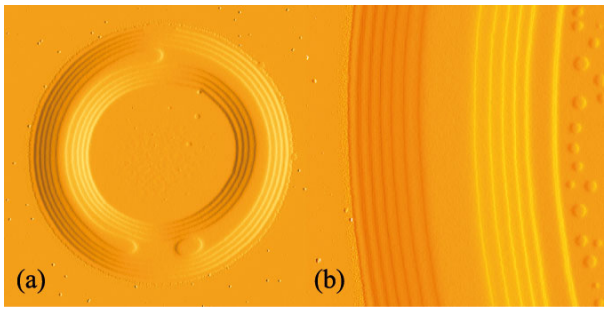

Fig. 2. a) AFM tapping amplitude of a copolymer ring that has been annealed at 180 °C for 2 hr; the image is 20 μm wide. b) A close up of another ring, a 10 μm scan.

radius so that the in-plane curvature is small, then we will show that it is possible to ignore the contribution of the edge tension to the change in free energy. Neglecting the edge tension simplifies the system significantly.

These samples provide an ideal geometry for the study of the edge interactions for two reasons. First, we can treat the system as 2-D with no change in the free energy due to edge tension. Second, once the the terraces develop (see fig. 1b)), the only interaction that drives changes in the morphology is the interaction between edges. In equilibrium all layers must be centred such that the stack is symmetric about the midpoint of the rim (*e.g.*, in fig. 1b), this corresponds to $(x_1 + x_6) = (x_2 + x_5) = (x_3 + x_4)$). By studying the evolution from the initial asymmetric edge distribution towards a symmetric one, it is possible to investigate the form of the repulsive interaction between edges.

2 Experiment

The ring samples were prepared using the method as described previously [33]. Briefly, a droplet of methanol covers the surface of a 1×1 cm^2 Si wafer (University Wafer). A small syringe (~ 0.5 mm diameter) filled with polymer dissolved in toluene is suspended just above the methanol bath. A small droplet of the polymer solution is allowed to fall into the methanol bath and spin coating at approximately 4000 rpm is immediately initiated. Here the polymer is soluble in toluene, and toluene is miscible with methanol. However, the polymer is not soluble in methanol. As the droplet of polymer solution falls into the methanol bath, the rapid shearing during spincoating breaks the drop into many tiny droplets, some of which land on the substrate. Toluene within these droplets exchanges with the methanol causing the diblock to precipitate and form rings [33]. With appropriate timing it is possible to find polymer ring sections scattered randomly over the substrate. Typical dimensions for the rings are approximately 200 nm in height, 50 μm in diameter and 5 μm wide, making them ideally suited for study by AFM (Veeco Caliber). In contrast with our previous work on the evolution of homopolymer rings [33], here a symmetric diblock copolymer, PS-PMMA, was used (Polymer

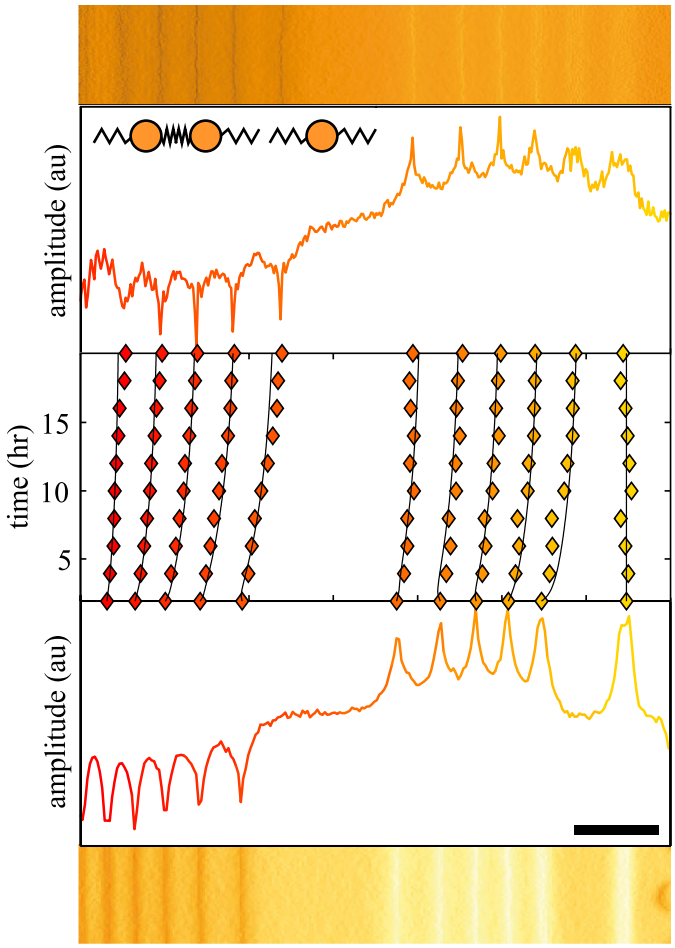

Fig. 3. From the bottom up: a portion of an AFM image as in fig. 2b) for $t = 2$ hr of annealing; its vertically averaged line profile; data points for the extrema which correspond to the lamellar edges from AFM scans after cumulative annealing times; the top two panels are analogous to the bottom two, except they are for data taken after $t = 20$ hr of annealing. The scale bar and separations between adjacent tick marks on the horizontal scale in the central portion are 1 μm wide. All portions of the figure have the same horizontal scale. The "spring-and-bead" schematic represents the mechanical system discussed in the text with the potential given by eq. (4).

Source Inc. Dorval, Canada). The total molecular weight was 46 kg/mol, with a polydispersity index of 1.05. Solutions of toluene and PS-PMMA were prepared with a polymer mass fraction of approximately 0.5%.

The ring samples supported on the Si substrate were placed on a heating stage (Linkam Scientific) and annealed at 180 °C for two-hour periods in ambient conditions. Prior to the first annealing step, polymers are in the disordered state and the rings are topographically indistinguishable from those of a homopolymer ring, as shown schematically in fig. 1a). After the first two-hour annealing step, the polymer chains phase separated into fully developed lamellar structures. The terrace edges were easily identified with the AFM tapping amplitude signal, as shown in figs. 2 and 3 (the AFM tapping amplitude or

error signal can be interpreted as roughly the gradient of the topography). The subsequent annealing steps allow us to gather time-dependent edge positions, $x_i(t)$ as defined in fig. 1a). The edge positions were determined by finding the extrema in the tapping amplitude line profiles (fig. 3).

To obtain the data presented in fig. 1c) of an isolated terrace edge, a thin film of PS-PMMA was spincast onto a 1×1 cm^2 Si wafer. The resulting film, prepared such that it was incommensurate with the lamellar spacing of the diblock, resulted in a surface perforated with holes upon annealing at 180°C for several hours. The holes were of various lateral sizes and had a constant depth corresponding to the height of a single bilayer, $H_o \sim 30$ nm. AFM in tapping mode was used to obtain topography data of holes with radii ranging from $2\,\mu$m to $7\,\mu$m (note that this is larger than the transition region between two lamellar terraces). Furthermore, all line profiles were taken perpendicular to the transition between the two lamellar teraces present at the air-polymer interface. Transition profiles, irrespective of the diameter of the holes studied, were identical and are shown in fig. 1c). The perturbation due to the transition from one terrace to the next ranges approximately $0.5\,\mu$m, which compares favourably with results of previous workers [26, 28, 29].

3 Experimental results

The perturbation induced by an edge results in a cost to the free energy as two edges approach one another [31]. Starting from the asymmetric distribution of the edges, the equilibrium configuration should result in a symmetric topography. In the central panel of fig. 3 the position of each edge is shown as a function of increasing time as the topography evolves. As expected, the last measurement at 20 hours of annealing is symmetric, with intermediate times providing the evolution of the edges. The ring observed contained $n = 12$ edges (six bilayer lamellae). In addition to the twelve bilayer edges, there is one edge in contact with the substrate. This edge corresponds to the monolayer carpet of molecules which forms because of the asymmetric wetting conditions of our experimental system (see fig. 1b)). During the course of the expriment, there is no observable change to this monolayer. Just as in earlier work on droplets [31], the monolayer position does not measurably affect the remaining lamellae in the stack. Thus, here we focus only on the stack of lamellae on top of the monolayer. The positions of the edges as shown in fig. 3 are always measured with respect to the bilayer edge furthest from the centre of the ring, *i.e.* $x_1 = 0$ as shown in fig. 1b).

Measurements of lamellar edge dynamics as shown in fig. 3 were made for multiple rings. The rings studied had five, six and seven bilayers, all with slightly different initial conditions. Due to the fabrication procedure, the ring profile always has a steep side facing the substrate and a shallower side facing the central portion of the ring, and the initial edge configurations are always similar to that shown schematically in fig. 1b). For all the rings studied, the data is qualitatively similar to that shown in fig. 3. To demonstrate this consistency, three additional edge trajectories from distinct rings with five or six bilayers are shown in fig. 4.

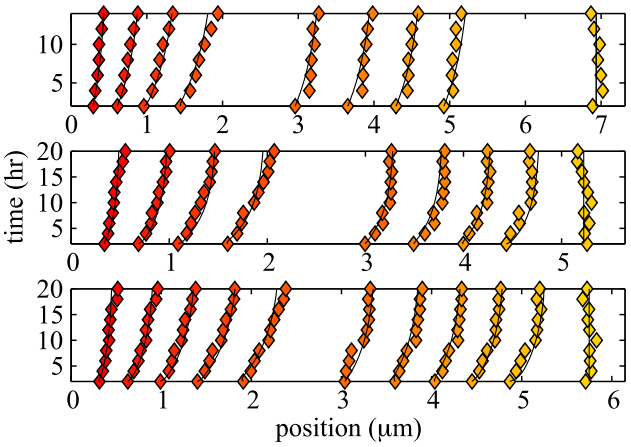

Fig. 4. Three plots of edge position as a function of annealing time for different rings. The black lines are best fits of the model described by eqs. (2), (3) and (4) to the experimental data.

4 Model

Figure 3 demonstrates that the configuration of lamellar edges is not static in time. Rather, there is an interplay of forces which causes them to move toward a state of lower free energy. To describe the evolution of these trajectories quantitatively, we resort to a simplified classical picture. We stress that in this tentative model we have not attempted to rigorously derive a molecular level description, as that currently eludes us. However, given the existence of an unfavourable repulsive interaction between edges, it is possible to elucidate the form of that interaction.

The model can be understood in its simplest terms from the following ingredients: 1) As is clear from fig. 2, there is little curvature of the edges in the lateral direction. Thus, the edge tension does not significantly contribute to changes in the free energy. 2) We assume that volume is conserved within the region that we are investigating. The validity of this is easily verified experimentally as discussed below. 3) While the molecular details are complex, we can think of the edges as being acted upon by a repulsive force. The edges move, while conserving volume, so as to minimise the total interaction. 4) The system is highly dissipative because of the viscous environment. While complex molecular mechanisms are at play, we model the dissipation in the simplest possible way: the velocity with which the edges move is proportional to the force acting upon them.

Before the details of the model are developed further, we provide a few more comments about the link between the simple classical model, and the real molecular system. Clearly, it is not the case that the edges represent

a rigid interface upon which a force acts, akin to pistons responding to a force in a viscous fluid. The molecules within each lamella exchange with neighbouring lamellae in response to a pressure or difference in potential. This exchange conserves volume, is dissipative, acts to minimize the free energy of the entire system, and should be taken as analogous to the simpler mechanical model we discuss here. It is the hope that a future detailed theoretical model, including the cost of the defects, can provide a more rigorous treatment.

In the simple classical picture, the energy of two adjacent lamellar edges is a function of the distance between them. For a given lamellar stack, as shown schematically in fig. 1, the total free energy is the sum of contributions from all pairs of edges,

$$\mathcal{F}(\{x_i\}) = F_o \sum_{i=1}^{n-1} g(w_i), \tag{1}$$

where $w_i = x_{i+1} - x_i$ is the distance between edges, F_o is a constant which sets the energy scale and n is the number of lamellar edges in the stack of $n/2$ bilayers. $g(w)$ is the function that describes how the free energy of two lamellar edges changes when they approach one another; only nearest neighbour edge interactions are taken into account. In principle the interaction between the edges that represent the top layer might have an interaction that differs from $g(w)$. For simplicity we have assumed this interaction to be of the same form.

The dissipation is included with an energy term of the form $\dot{W}_i = -\zeta \dot{x}_i^2/2$ [37], where ζ is a constant and the dot denotes differentiation with respect to time. As stated above, we limit ourselves to systems where the volume is conserved. In fact, material flows tangentially along the rings, changing the volume within the cross-section of the ring studied. A clear example of significant tangential flow is shown in fig. 5. However the flow on this larger length scale occurs on a longer time scale than that for which we apply the model. Conservation of volume is equivalent to stating that the sum of the lamellar widths is constant. That is, $\mathcal{L} = \sum_{i=1}^{n/2}(x_{n-i+1} - x_i)$ remains constant. Multiplying $\mathcal{L}$ by H_o gives the area of the stack, and so $\mathcal{L}H_o$ can be seen as the differential volume element of the ring. Strictly speaking, the edge perturbs the thickness of the lamellae near the edge (see fig. 1c)) which accounts for the flow around the circumference of the ring which breaks up into individual droplets (fig. 5). The morphology is reminiscent of the Plateau-Rayleigh instability observed in our previous work on homopolymer rings [33], although the mechanism for the development of the morphology in the symmetric diblock case is much more complex. Barnard and co-workers have observed similar layered structures prepared with dendrimers [35,36].

The system under consideration is highly viscous and we assume that inertial effects play a negligible role in the evolution of the lamellar stacks. With this assumption and using eq. (1) along with the constant volume constraint, the Euler-Lagrange equations predict the classical trajectories of lamellar edges:

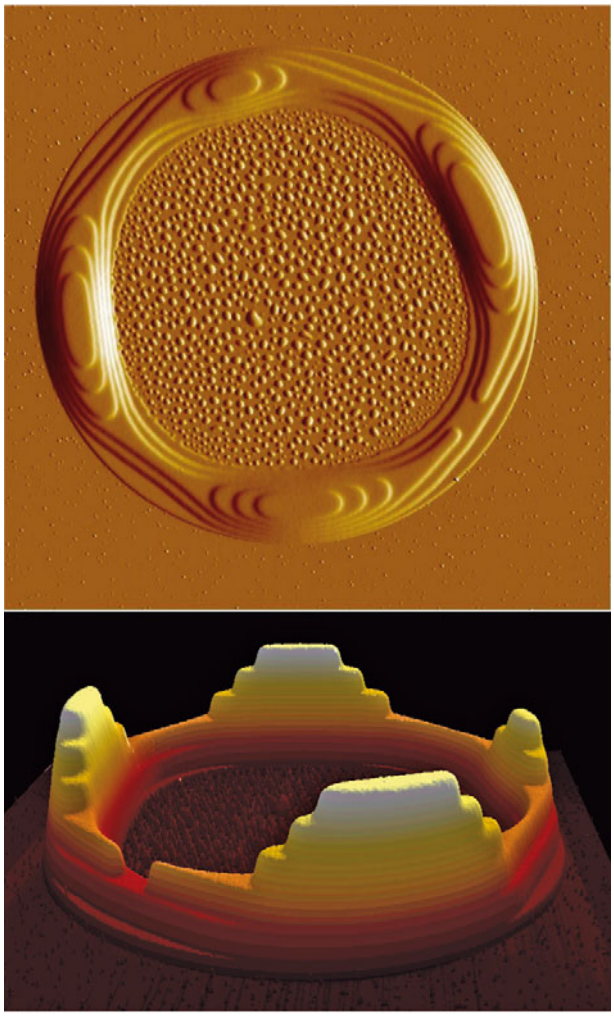

Fig. 5. AFM tapping amplitude (top) and topography (bottom) signal of a diblock ring in the late stages of annealing. A Plateau-Rayleigh-like instability has developed and the ring is showing the formation of four distinct droplets. The scan area is approximately $54 \times 54\,\mu\mathrm{m}^2$.

$$\frac{Q\dot{x}_i}{w_o^2} = g'(w_{i-1}) - g'(w_i) \pm \tau, \tag{2}$$

$$\tau = \frac{1}{n-2}\left[g'(w_1) + g'(w_{n-1}) - 2g'(w_{n/2})\right]. \tag{3}$$

Here, $Q = w_o^2\zeta/F_o$ is the time scale of the system, w_o sets the range of the interaction. Furthermore, τ is the Lagrange multiplier introduced by the constraint of constant volume. The first two terms result from the condition $\dot{x}_1 = \dot{x}_n = 0$ which we impose based on our experimental data. The Lagrange multiplier represents the difference in net forces acting on the left- and right-hand sides of the lamellar stack.

To compare the model to experimental data, we need to choose the potential, $g(w_i)$, in eq. (1). As demonstrated in [31] and [32], the approach of two lamellar edges forces chains to deviate from their preferred lamellar structures

and must cause a rise in the free energy. The potential, $g(w_i)$, describes that interaction. We assume that the potential is a monotonically decreasing function of the distance between the lamellae. In [31], an exponential form was assumed for analytical convenience, however that experiment was sensitive to the strength but not the form of the interaction. We have found that an exponential form does not describe the evolution of the edges acceptably. Here we propose a simple potential that gives rise to a distance-dependent repulsion: a truncated quadratic potential of the form

$$g(w_i) = \begin{cases} \left(1 - \frac{|w_i|}{w_o}\right)^2, & \text{if } |w_i| \leq w_o, \\ 0, & \text{otherwise.} \end{cases} \quad (4)$$

This functional form is appealing as it is a purely repulsive Hookean potential which smoothly drops to zero when the distance between edges increases to $|w_i| = w_o$ (as depicted by the bead-and-spring schematic in fig. 3). With an initial condition supplied to eq. (2), it is possible to compute edge trajectories using the potential described in eq. (4). The trajectories were computed for various values of w_o and Q, using a fourth-order Runge-Kutta algorithm.

5 Discussion

As seen in figs. 3 and 4, the model provides a good fit to the experimental data with $w_o = 0.49 \pm 0.02$ μm and $Q = 0.5 \pm 0.2$ hr. We note that the fits are strongly dependent on the length scale, but less sensitive to the time scale. The uncertainties reflect the statistical distribution of the best fitting parameters of our nine measured edge trajectories (four of which are shown in figs. 3 and 4). In selecting rings to analyze, we have discarded any data that do not satisfy the constant volume constraint described in sect. 4. Thus, whenever the net circumferential flux of molecules at the point of measurements becomes non-zero, we cease consideration of the data set. For this reason the time scales in fig. 4 are not all the same.

Having demonstrated that the model is consistent with the data, we now discuss some implications and limitations of the analysis and experiment. The results presented provide further credence to the idea that the edges of diblock copolymer terraces *repel* one another. Furthermore, the data is sensitive to the chosen potential. While we have tried to model the data using an exponential potential (as in [31]) it was not possible to obtain acceptable fits for all data sets. Additionally, even only considering data sets for which acceptable fits were possible using the exponential potential, the fit parameters were not consistent with one another. In contrast, the Hookean form of the repulsion provided satisfactory fits to multiple rings with a range of initial conditions while the *two* fitting parameters were consistent for each case.

As discussed, the quadratic potential does not capture the complete picture: 1) While the Hookean model is appealing for its simplicity and consistent with experimental results, we cannot exclude the possibility of other forms of the interaction which may also provide satisfactory results. 2) We have not considered molecular level details, but have instead attempted to give a minimal description which captures the essence of the problem. The potential described by eq. (4) is purely repulsive for edge separations less than w_o. One can compare the value of w_o as determined from best fits of the dynamical edge trajectories, $w_o \sim 0.5$ μm, to the profile width of isolated edges as shown in fig. 1c). From the figure it is clear that the lengthscale over which the presence of an isolated edge relaxes away is similar to w_o. Clearly a repulsive interaction cannot exist until these perturbed regions between two edges overlap. To put it another way, it is the profile width of isolated edges in equilibrium that controls the dynamic response of interacting lamellar edges. This comparison gives a consistency which provides further support for the proposed model.

The time scale is set by the parameter $Q = w_o^2\zeta/F_o$. Thus, having obtained the best fit values for the distance and time scales, we can determine the ratio of the driving force and the dissipation. That is, $F_o/\zeta = w_o^2/Q \approx 10^{-12}$ cm^2/s. While dimensionally like a diffusion constant, the process we have investigated in this study is driven, so care must be taken in direct comparisons to diffusion of diblocks. The dynamics of diblock copolymers have been discussed by many authors in the past and diffusion coefficients for a variety of diblock copolymers span a broad range of values including 10^{-12} cm^2/s [38–40].

6 Conclusion

Understanding topological defects, and the interplay between them, underpins the control of morphologies. Here we have used the simplest form of soft confinement, that is, the confinement induced by a free interface, to investigate the interaction between steps in lamellae formed by a symmetric diblock copolymer. The underlying bilayer structure responds to a continuously varying topography by forming terraces — steps which correspond to the height of one bilayer. If the variation in the height is steep enough, then the terrace edges form close to one another, and the edge defects interact via a long-range repulsion. While the molecular details remain elusive, the source of the repulsion is intuitive: an edge is a defect which perturbs the surface profile with an associated cost to the surface energy. As two isolated edges approach, the perturbation deviates further, thereby deforming the equilibrium edge structure and increasing the free energy. We have performed measurements of the dynamics of interacting edges in structures with an asymmetric topography which, for all practical purposes, varies only in one dimension. These structures are nanoscale rims that form on a substrate much like the rim left by a coffee stain [33–36]. The asymmetric shape of the rim's cross-section, steep towards the outside of the ring and shallow towards the middle, ensures that the steps associated with the terraces have various distances between them. However, when only

the repulsive interaction of the edges is present the equilibrium morphology must be symmetric. By monitoring the evolution towards that symmetric structure one can elucidate the nature of the repulsive interaction using a simple classical model: in a dissipative system, the rate of change in the position of an edge is proportional to the force acting upon it, which in turn is dependent on the gradient of the repulsive potential. Here we have found that a Hookean repulsion between the edges is in good agreement with the data. While we cannot exclude the existence of other equally successful repulsive interactions, the best fit parameters provide additional evidence for a Hookean form. Specifically, the width over which the interaction acts is of the same length scale as the equilibrium perturbation of an interface by an isolated lamellar edge.

The authors thank Professor A.-C. Shi for valuable discussions. Financial support from NSERC of Canada is gratefully acknowledged.

References

1. M.W. Matsen, J. Phys.: Condens. Matter **14**, R21 (2002).
2. G. Strobl, *The Physics of Polymers: Concepts for Understanding their Structures and Behaviour*, 3rd edn. (Springer, 2007).
3. A.K. Khandpur, S. Förster, F.S. Bates, I.W. Hamley, A.J. Ryan, W. Bras, K. Almdal, K. Mortensen, Macromolecules **28**, 8796 (1995).
4. T. Thurn-Albrecht, J. Schotter, G.A. Kästle, N. Emley, T. Schibauchi, L. Krusen-Ebaum, K. Guarini, K.T. Black, M.T. Tuominen, T.P. Russell, Science **290**, 2126 (2000).
5. C. Tang, E.M. Lennon, G.H. Fredrickson, E.J. Kramer, C.J. Hawker, Science **322**, 429 (2009).
6. C. Creton, E.J. Kramer, H.R. Brown, C.Y. Hui, Adv. Polym. Sci. **156**, 53 (2002).
7. I.W. Hamley, Progr. Polym. Sci. **34**, 1161 (2009).
8. E. Helfand, J. Chem. Phys. **62**, 999 (1975).
9. F.S. Bates, Science **251**, 898 (1991).
10. M.W. Matsen, F.S. Bates, Macromolecules **29**, 1091 (1996).
11. D.S. Herman, D.J. Kinning, E.L. Thomas, L.J. Fetters, Macromolecules **20**, 2940 (1987).
12. H. Hirokazu, H. Tanaka, K. Yamasaki, T. Hashimoto, Macromolecules **20**, 1651 (1987).
13. G.H. Fredrickson, Macromolecules **20**, 2535 (1987).
14. M. Foster, M. Sikka, N. Singh, F. Bates, S. Satija, C. Majkrzak, J. Chem. Phys. **96**, 8605 (1992).
15. A. Menelle, T. Russell, S. Anastasiadis, S. Satija, C. Majkrzak, Phys. Rev. Lett. **68**, 67 (1992) ISSN 1079-7114.
16. K. Shull, Macromolecules **25**, 2122 (1992) ISSN 0024-9297.
17. H. Tan, D. Yan, A. Shi, Macromolecules **37**, 9646 (2004).
18. P. Lambooy, T.P. Russell, G.J. Kellogg, A.M. Mayes, P.D. Gallagher, S.K. Satija, Phys. Rev. Lett. **72**, 2899 (1994).
19. W. Li, R.A. Wickham, R.A. Garbary, Macromolecules **39**, 806 (2006).
20. B. Yu, P. Sun, T. Chen, Q. Jin, D. Ding, B. Li, A.C. Shi, Phys. Rev. Lett. **96**, 138306 (2006).
21. P. Chen, H. Liang, A.C. Shi, Macromolecules **41**, 8938 (2008).
22. P. Dobriyal, H. Xiang, M. Kazuyuki, J.T. Chen, H. Jinnai, T.P. Russell, Macromolecules **42**, 9082 (2009).
23. M. Ma, E.L. Thomas, G.C. Rutledge, B. Yu, B. Li, Q. Jin, D. Ding, A.C. Shi, Macromolecules **43**, 3061 (2010).
24. B. Collin, D. Chatenay, G. Coulon, D. Ausserre, Y. Gallot, Macromolecules **25**, 1621 (1992).
25. P. Green, R. Limary, Adv. Colloid Interface Sci. **94**, 53 (2001).
26. M. Maaloum, D. Auserre, D. Chatenay, G. Goulon, Y. Gallot, Phys. Rev. Lett. **68**, 1575 (1992).
27. K. Niihara, U. Matsuwaki, N. Torikai, K. Satoh, M. Kamigaito, H. Jinnai, Polym. J. **39**, 1105 (2007).
28. B.L. Carvalho, E.L. Thomas, Phys. Rev. Lett. **73**, 3321 (1994).
29. Y. Liu, M.H. Rafailovich, J. Sokolov, S.A. Schwarz, S. Bahal, Macromolecules **29**, 899 (1996).
30. A. Horvat, A. Knoll, G. Krausch, L. Tsarkova, K.S. Lyakhova, G.J.A. Sevink, A.V. Zvelindovsky, R. Magerle, Macromolecules **40**, 6930 (2007).
31. A.B. Croll, M.V. Massa, M.W. Matsen, K. Dalnoki-Veress, Phys. Rev. Lett. **97**, 204502 (2006).
32. J.U. Kim, M.W. Matsen, Soft Matter **5**, 2889 (2009).
33. J.D. McGraw, J. Li, D.L. Tran, A.C. Shi, K. Dalnoki-Veress, Soft Matter **6**, 1258 (2010).
34. R. Deegan, O. Bakajin, T. Dupont, G. Huber, S. Nagel, T. Witten, Nature **389**, 827 (1997).
35. F.I. Li, P.H. Leo, J.A. Barnard, J. Phys. Chem. B **112**, 16497 (2008).
36. F.I. Li, P.H. Leo, J.A. Barnard, J. Phys. Chem. C **112**, 14266 (2008).
37. H. Goldstein, *Classical Mechanics*, 2nd edn. (Addison-Wesley, 1980).
38. H. Yokoyama, Mater. Sci. Eng. R **53**, 199 (2006).
39. G.H. Fredrickson, F.S. Bates, Annu. Rev. Mater. Sci. **26**, 501 (1996).
40. T.P. Lodge, M.C. Dalvi, Phys. Rev. Lett. **75**, 657 (1995).